DR WEI SUN (Orcid ID : 0000-0001-5675-0466)

Article type : Original Article

Corresponding author mail id: slchen@icmm.ac.cn

The medicinal plant *Andrographis paniculata* genome provides insight into biosynthesis of the bioactive diterpenoid neoandrographolide

Wei Sun[1*] Liang Leng[1*] Qinggang Yin[1*] MeiMei Xu[2*] Mingkun Huang[1] Zhichao Xu[3] Yujun Zhang[1] Hui Yao[3] Caixia Wang[1] Chao Xiong[1] Sha Chen[1] Chunhong Jiang[4] Ning Xie[4] Xilong Zheng[5] Ying Wang[6] Chi Song[1#] Reuben J. Peters[2#] Shilin Chen[1#]

1. Key Laboratory of Beijing for Identification and Safety Evaluation of Chinese Medicine, Institute of Chinese Materia Medica, China Academy of Chinese Medical Sciences, Beijing, China

2. Roy J. Carver Department of Biochemistry, Biophysics and Molecular Biology, Iowa State University, Ames, IA 50011-1079, USA

3. Institute of Medicinal Plant Development, Chinese Academy of Medical Sciences & Peking Union Medical College, Key Laboratory of Bioactive Substances and Resources Utilization of Chinese Herbal Medicine, Ministry of Education, Beijing, China

4. State Key Laboratory of Innovative Natural Medicine and TCM Injections, Jiangxi Qingfeng Pharmaceutical Co. Ltd.

5. Hainan Branch Institute of Medicinal Plant Development Chinese Academy of Medical Sciences, Wanning, China

6. Wuhan Benagen Tech Solutions Company Limited, Wuhan 430070, China

Chi Song, Reuben Peters and Shilin Chen are corresponding co-authors

This article has been accepted for publication and undergone full peer review but has not been through the copyediting, typesetting, pagination and proofreading process, which may lead to differences between this version and the Version of Record. Please cite this article as doi: 10.1111/tpj.14162

Running title: Andrographis paniculata genome sequence

Keywords: Genome sequence, Andrographis paniculata, Diterpenoid, TPS, Glucosyltransferase

Summary

Andrographis paniculata is a herbaceous dicot plant widely used for its anti-inflammatory and anti-viral properties across its distribution in China, India and other Southeast Asia countries. *A. paniculata* was used as a crucial therapeutic treatment during the influenza epidemic of 1919 in India and is still used for the treatment of infectious disease in China. *A. paniculata* produces large quantities of the anti-inflammatory diterpenoid lactones andrographolide, neoandrographolide and their analogs; touted to be the next generation of natural anti-inflammatory medicines for lung diseases, hepatitis, neurodegenerative disorders, autoimmune disorders and inflammatory skin diseases. Here, we report a chromosome-scale *A. paniculata* genome sequence of 269 Mb that was assembled by Illumina short reads, PacBio long reads and Hi-C data. Gene annotation predicted 25,428 protein-coding genes. To decipher the genetic underpinning of diterpenoid biosynthesis, transcriptome data from seedlings elicited with methyl jasmonate also was obtained, which enabled identification of genes encoding diterpenoid synthases, cytochrome P450 monooxygenases, 2-oxoglutarate-dependent dioxygenases and UDP-dependent glycosyltransferases potentially involved in diterpenoid lactone biosynthesis. We further carried out functional characterization of pairs of classes I and II diterpene synthases, revealing the ability to produce diversified labdane-related diterpene scaffolds. In addition, a glycosyltransferase able to catalyze O-linked glucosylation of andrograpanin, yielding the major active product neoandrographolide, was identified as well. Thus, our results demonstrate the utility of the combined genomic and transcriptomic dataset generated here for investigation of the production of the bioactive diterpenoid lactone constituents of the important medicinal herb *A. paniculata*.

Introduction

Since the dawn of human kind, humans have utilized botanical medicines for the treatment of ailments (Roy Upton, 2015). There is high demand for herbal medicines in developing countries due to its perceived effectiveness, cultural acceptability, and affordability (Pal and Shukla, 2003; Kamboj, 2000). Most herbal medicines originated from traditional therapeutic theory and the practice can be dated back before the development and spread of modern medicine. With advancement of the field of phytochemistry, focus shifted away from the plant material itself and towards the isolated active compounds (Roy Upton, 2015). Some single-ingredient modern drugs and dietary supplements are derived directly or indirectly from plants including: artemisinin (from *Artemisia annua* L.), podophyllotoxin (from *Podophyllum peltatum* L.), paclitaxel (from *Taxus brevifolia* Nutt.), vincristine (from *Catharanthus roseus*) and morphine (from *Papaver somniferum* L.) (Raskin *et al.*, 2002; Goel *et al.*, 2008). Meanwhile, prescriptions of herbal

medicines involve the simultaneous action of multiple constituents of the plant part as a whole, thought to act synergistically by hitting many molecular targets, or a single target (Li and Weng, 2017). Currently in China both herbal plant material and modern chemically characterized drugs are prescribed.

Andrographis paniculata (Burm. f.) Nees **(Fig. 1)** is a member of the order Lamiales, Acanthaceae (family), widely distributed and utilized in tropical and sub-tropical regions of Asia, including India, China, Thailand, and Malaysia (Lim *et al.*, 2012). Its use across this region is well known and historically documented in both traditional Chinese medicine (TCM) and the Ayuveda system in India (Anju *et al.*, 2012; Pholphana *et al.*, 2013). It is known as "Chuanxinlian" in Chinese and Kalmegh in India, which expresses its strong bitter taste. In North India, *A. paniculata* is known as Maha-tikta; literally meaning "king of bitters" (Benoy *et al.*, 2012; Subramanian *et al.*, 2012). Its medicinal uses have included a variety of inflammation diseases such as diarrhea, fevers, laryngitis, gastric infections, upper respiratory tract infections, as well as other chronic and infectious disorders (Lim *et al.*, 2012). *A. paniculata* has been included in the "WHO monographs on selected medicinal plants (World Health Organization, 2002), where it was reported that the plant was considered highly efficacious in inhibiting the spread of the influenza epidemic of 1919 in India (Amroyan *et al.*, 1999; Sudhakaran, 2012; Avani and Rao, 2008; Sc, 2014; Lim *et al.*, 2012). Phytochemical data shows that *A. paniculata* can produce high quantities of biologically active *ent*-labdane-type diterpenoids and flavones, such as andrographolide, neoandrographolide and andrographidine A, B, C (Subramanian *et al.*, 2012; Ma *et al.*, 2010; Koteswara Rao *et al.*, 2004; Chao and Lin, 2010; Wang *et al.*, 2009). The main bioactive compounds andrographolide and neoandrographolide are derived from the *ent*-copalol (*ent*-labda-8(17),13-dien-15-ol) diterpene backbone. This undergoes two regio-specific oxygenations, at C16 and C19, as well as heterocyclization to a 16,15-lactone, to form andrograpanin. Neoandrographolide is produced from this aglycone by glucosylation at the C19-hydroxyl, while andrographolide is formed by two further hydroxylations at C3 and C14. Modern pharmacological evidence suggests that *A. paniculata* as well as its diterpenoid constituents has anti-inflammatory, antimalarial, anticancer, immunomodulatory, antidiabetic and other effects (Singha *et al.*, 2003; Ajaya Kumar *et al.*, 2004; Reyes *et al.*, 2006; Sheeja *et al.*, 2006; Chandrasekaran *et al.*, 2010). This efficacy against inflammatory diseases has translated to a wide range of medical applications of *A. paniculata* in China and India.

Despite the medical importance of *A. paniculata*, in part due to the lack of a genome sequence, the pathways for biosynthesis of the bioactive diterpenoids such as andrographolide and neoandrographolide remain largely unknown. Here, we present a high-quality genome for *A. paniculata*, with contig N50 of 388 Kb, assembled using Pacbio SMRT long reads. Hi-C technology was then used to anchor more than 95 percent of this sequence to 24 pseudo-chromosomes. Based on mining of this genome sequence, as well as transcriptomic sequence data generated from different tissues and MeJA treated seedlings, we describe the *in vitro* functional characterization of four members of the *A. paniculata* diterpene synthase family and uncover the encoded diversity of labdane-related diterpene backbones. Additionally, we biochemically screened nine glycosyltransferases and found one that catalyzes conversion of andrograpanin to neoandrographide *in vitro* as well.

Results and discussion

Genome sequencing and assembly

Both flow cytometry and *k*-mer analysis were utilized for estimating the size of the *A. paniculata* genome prior to whole genome sequencing. Flow cytometry gave an estimated haploid genome size of 280 Mb, while *k*-mer analysis yielded a very similar estimate of 281.26 Mb (**Supplementary Fig. 1-2**). We used Pacbio SMRT long-read sequencing to assemble the *A. paniculata* genome **(Supplementary Table 1)**. The size of the assembled genome was ~269 Mb, with 1,278 contigs (longest of 2.07 Mb) and a contig N50 of 388 Kb **(Table 1)**. Nearly all contigs have a length more than 10 Kb, and 23 contigs (1.8%) have a length over 1 Mb. The contig N50 of this Pacbio-only assembly is comparable or even better than recently finished plant genomes assembled with both Illumina and Pacbio reads **(Supplementary Table 2)**. We further generated ~270 million Illumina paired-end reads (40.2 Gb), more than 96 percent of which could be mapped to this *A. paniculata* draft genome. In addition, we generated transcriptomes assembled from Illumina RNA-seq reads and mapped them to the draft genome. Of the 40,046 transcripts >1000 bp, 35,413 (88.43%) could be mapped to a single scaffold with >90% sequence coverage, and 38,376 (95.83%) could be mapped with >50% sequence coverage (**Supplementary Table 3**). BUSCO (Benchmarking Universal Single-Copy Orthologs) analysis was also used to estimate completeness of genome assembly and 89.4 % (271/303) of eukaryote gene sets were classified as complete **(Supplementary Table 3)**. These results indicated successful assembly of the major genic regions of the *A. paniculata* genome. Hi-C technology was then used to anchor contigs to pseudo-molecules (**Supplementary Fig. 3**). More than 95 percent (257 Mb) of the assembled contigs could be anchored to 24 pseudo-chromosomes **(Supplementary Table 4)**, with maximum and minimum lengths of 14.7 Mb and 7.7 Mb, respectively.

A. paniculata genome annotation and evolution

The *A. paniculata* genome was annotated by a combination of *ab initio*, homology-based and RNA-Seq assembly-based analyses. This led to prediction of 25,428 protein-coding genes, with an average exon number of 5.79, transcript length of 3,412 bp and CDS length of 1,255bp (**Supplementary Table 5**). We then compared these genes with that of related species (Fig. 2A, B). The number of gene families in *A. paniculata* (12,072) is similar to that in other plants – e.g. *Sesamum indicum* (13,247), *Arabidopsis thaliana* (13,076), and *Utricularia gibba* (11,513) **(Supplementary Table 6)**. We found a total of 587 families were *A. paniculata* specific when compared to the genomes of *Vitis vinifera*, *Solanum lycopersicum* and *Solanum tuberosum* **(Fig. 2A; Supplementary Table 7**). The divergence of *A. paniculata* and 11 other plants, based on their genomes, was estimated from 305 one-to-one orthologous genes **(Fig. 2C)**, with the split between *A. paniculata* and the ancestor of *Mimulus guttatus* and *S. indicum* estimated to be approximately 58.8 Myr ago. Gene gain-loss was analyzed for *A. paniculata* relative to these 11 other species. In the *A. paniculata* lineage 5,383 gene families appear to be undergoing contraction, while one quarter of this number (1,290) appear to be expanding **(Fig. 2D)**. Genes in these expanded families were annotated by InterProScan, followed by functional enrichment analysis of these

genes (**Supplementary Table 8**). Interestingly, among these were the terpene synthase (TPS) (IPR001906, P=0.00013) and cytochrome P450 (CYP) monooxygenase (IPR001128, P=0.00043) families, which are important in secondary metabolism such as that leading to andrographolide and neoandrographolide.

Repetitive sequences were identified using a combination of *ab initio* and homology-based approaches. There appear to be fewer repeat elements in *A. paniculata* (53.3% of assembly) than *S. lycopersicum* (63.2%) and *S. tuberosum* (54.5%), but more than *S. indicum* (28.5%) and *V. vinifera* (41.4%). The two most numerous types of long terminal repeat (LTR) retrotransposons in *A. paniculata* are Ty3/Gypsy-like LTRs (10.54%) and Ty3/Copia-like LTRs (8.42%) (**Supplementary Table 9**). Synonymous substitution rates (K_s) among paralogues and orthologues were calculated to explore possible paleopolyploidy in the *A. paniculata* genome. This analysis indicates that *A. paniculata*, *S. lycopersicum S. indicum* and *V. vinifera* share one paleopolyploid event, referred to as the paleohexaploidy (γ) event common to all eudicots (**Supplementary Fig. 4**) (Tang *et al.*, 2008; Vekemans *et al.*, 2012). After the split of *A. paniculata* and *S. indicum* (~ 59 million years, Fig. 2C), *S. indicum* and *S. lycopersicum* each experienced a lineage specific WGD (Wang *et al.*, 2014; Tomato Genome Consortium, 2012), but no clear peak could be seen in *A. paniculata* (**Supplementary Fig. 4**). These results jointly imply that *A. paniculata* did not undergo WGD after its split with *S. indicum*.

A. paniculata diterpenoid profiles

To correlate *A. paniculata* diterpenoid metabolism with gene expression, transcriptome (RNA-Seq) analysis was carried out for seedlings treated with methyl jasmonate (MeJA). This mimics the wounding response and induces such secondary metabolism. In addition, the content of nine diterpenoid lactones was also targeted for analysis in these induced seedlings by ultra-high-performance liquid chromatography coupled with triple quadrupole tandem mass spectrometry (UHPLC/MS/MS) **(Table 2)**. Among these, 14-deoxyandrographolide, andropanolide and andrographolide were the predominant metabolites found. The aglycone of neoandrographolide, andrograpanin was only found in trace amounts compared to neoandrographolide, indicating highly efficient glucosylation. All detected diterpenoids exhibited increases relative to control plants, indicating that MeJA induces their production (Jian and Wu, 2005; Chen *et al.*, 2007; Chen *et al.*, 2006; Kim *et al.*, 2006; Wang *et al.*, 2010).

Diterpenoid backbone biosynthesis

Terpenoids are derived from isopentenyl diphosphate (IPP) and dimethylallyl diphosphate (DMAPP) precursors synthesized in plants by the mevalonate (MVA) pathway in the cytosol, or the 2-C-methyl-D-erythritol-4-phosphate (MEP) pathway in the plastids (Vranová *et al.*, 2013). The formation of the general diterpenoid precursor (*E*,*E*,*E*)-geranylgeranyl diphosphate (GGPP) involves via coupling of IPP to DMAPP by the action of GGPP synthases (GGPPS) (Ma *et al.*, 2012). From the genome assembly, fifteen genes were predicted to be involved in the MVA pathway and fourteen genes for the MEP pathway, along with thirteen GGPPS-like genes, all found using the KEGG database (Kanehisa and Goto, 2000)(**Supplementary Table 10**). Notably, at least one gene for each enzyme in the MEP and MVA

pathways showed increased transcript levels following MeJA treatment (**Supplementary Table 11**). The plastidial MEP pathway supplies the precursors for plant diterpene biosynthesis (Lange *et al.*, 2000). Among the relevant genes identified here from *A. paniculata* are those encoding five DXS (1-deoxy-D-xylulose 5-phosphate synthases), two HDR (4-hydroxy-3-methylbut-2-enyl diphosphate reductase), two HDS (4-hydroxy-3-methylbut-2-enyl diphosphate synthase) and two DXR (1-deoxy-D-xylulose 5-phosphate reductoisomerase), with one each of MCT (2-C-methyl-D-erythritol 4-phosphate cytidylyltransferase), CMK [4-(cytidine 5' diphospho)-2-C-methyl-D-erythritol kinase], MDS (2-C-methyl-D-erythritol 2,4-cyclodiphosphate synthase), indicating that genes encoding all seven MEP pathway enzymes have been identified. Protein subcellular localization prediction of these MEP pathway genes indicates that the encoded enzymes are most likely located in chloroplasts, further supporting their role in diterpenoid biosynthesis (**Supplementary Table 11**). In addition, while transcripts for most of the GGPPS-like genes were not significantly expressed in the analyzed tissues, four did appear to be up-regulated after MeJA treatment ($P < 0.001$) (**Supplementary Table 11**). These results suggest that the encoded enzymes might be involved in the production of andrographolide and related diterpenoids.

The bioactive diterpenoid lactones from *A. paniculata* fall into the labdane-related superfamily, whose biosynthesis is characterized by initial bicyclization of GGPP by a class II diterpene cyclase (Zi, Mafu, *et al.*, 2014). These most often produce copalyl/labdadienyl diphosphate (CPP), and are then termed CPP synthases (CPSs) **(Fig. 3)**. The resulting bicycles generally undergo further cyclization and/or rearrangement catalyzed by class I diterpene synthases, which are termed kaurene synthase-like (KSL) based on their homology to the *ent*-kaurene synthases found in all vascular plants for gibberellin phytohormone biosynthesis (Zi, Mafu, *et al.*, 2014) **(Fig. 3)**. Despite their distinct catalytic activity, CPSs and KSLs are phylogenetically related, falling into the larger terpene synthase (TPS) family, reflecting an ancient gene fusion event, and form the TPS-c and TPS-e sub-families, respectively (Chen *et al.*, 2011). To investigate the labdane-related diterpenoid biosynthetic capacity of *A. paniculata*, we mined its genome for CPSs and KSLs, much as previously reported for *Salvia miltiorrhiza* (Xu *et al.*, 2016; Ma *et al.*, 2012). In total, five putative CPSs and two putative KSLs were found. Of the CPSs (ApCPS1-5) only three (ApCPS1-3) appeared to be full-length and contained the characteristic DxDD aspartate-rich motif, while both KSLs (ApKSL1 & 2) appeared to be complete and contained the characteristic DDxxD motifs (**Supplementary Figures 5 and 6; Supplementary Tables 10 and 11**). Phylogenetic analysis of the translated protein with other previously functional characterized CPS and KSLs showed the expected grouping of CPS1-4 and ApKSL1 & 2 with class II and class I diterpene cyclases/synthases, respectively (**Fig. 4A and Supplementary Table 12**).

ApCPS2 has been previously characterized to function as an *ent*-CPP synthase (Misra *et al.*, 2015). The full-length CPSs newly identified here, ApCPS1 & 3, were functionally characterized by incorporation into a previously described modular metabolic engineering system (Cyr *et al.*, 2007). This enabled analysis by expression in *Escherichia coli* also engineered to produce GGPP. Both ApCPS1 & 3 were found to produce CPP, of either *ent*- or normal stereochemistry, as indicated by detection of the dephosphorylated derivative, copalol, from these cultures by GC-MS **(Fig. 4B)**. To ascertain the absolute configuration of their products, these were co-expressed with class I diterpene synthases specific for either normal CPP – i.e., a mutant of the bifunctional abietadiene synthase from *Abies grandis* that cannot produce CPP (Peters *et al.*, 2001), simply termed here AS – or for *ent*-CPP – i.e., the *ent*-kaurene synthase from *A. thaliana* (Yamaguchi *et al.*,

1998), simply abbreviated here as KS. The resulting products were then compared with those generated by CPSs of known stereospecificity as previously described (Cyr *et al.*, 2007). Notably, ApCPS1 produces both *ent*- and normal CPP, as demonstrated by its ability to supply substrate to both AS and KS **(Fig. 4C)**. This represents the first native class II diterpene cyclase with such clearly mixed stereochemical product outcome. By contrast, ApCPS3 is stereospecific, only producing CPP of normal stereochemistry **(Fig. 4D)**, as is more typically found with these enzymes (Peters, 2010; Zi, Matsuba, *et al.*, 2014).

While the characteristic DxDD motif acts as the catalytic acid (Prisic *et al.*, 2007), previous work with class II diterpene cyclases has highlighted the importance of the pair of residues that act as the catalytic base in determining product outcome. In particular, it has been noted that the CPSs that produce *ent*-CPP for production of the gibberellin phytohormones contain a conserved histidine and asparagine that form this catalytic dyad (Potter *et al.*, 2014). These two residues are conserved in both ApCPS1 & 2. This is consistent with the previously reported selective production of *ent*-CPP by ApCPS2 (Misra *et al.*, 2015), but is perhaps somewhat surprising for ApCPS1 given the mixture of *ent*- and normal CPP it was shown to produce here. Neither of these residues is conserved in ApCPS3, which selectively produces normal CPP. This is consistent with previous studies that have found an alternative pair of residues acting as the catalytic base, at least in normal CPP producing bifunctional diterpene synthases from gymnosperms (Criswell *et al.*, 2012; Mafu *et al.*, 2015).

The full-length KSLs identified here, ApKSL1 & 2, were similarly functionally characterized by incorporation in the same modular metabolic engineering system. In this case, by co-expression in *E. coli* also engineered to produce either normal, *ent*- or *syn*-CPP, as previously described (Cyr *et al.*, 2007). ApKSL1 was found to react specifically with normal CPP **(Fig. 4E)**, and produce the same mixture of abietadienes previously reported with AS (Peters *et al.*, 2000). On the other hand, ApKSL2 acted on both *ent*-CPP, producing *ent*-kaurene **(Fig. 4F)**, and normal CPP, producing isopimara-7,15-diene **(Fig. 4G)**. However, it should be noted that ApKSL2 seems to react more readily with normal, rather than *ent*-CPP, as indicated by the co-production of *ent*-copalol, which is derived from the ability of the endogenous dephosphatases to efficiently compete with ApKSL2 for *ent*-, but not normal, CPP. Thus, it must be noted that neither of these ApKSLs produces the expected *ent*-copalol or *ent*-labdatriene precursor to andrographolide and related diterpenoids. Given the recently reported finding that terpene synthases from the plant TPS-b sub-family can act upon CPP (Hansen *et al.*, 2016; Inabuy *et al.*, 2017), it seems at least possible that the *ent*-copalol/labdatriene synthase may be found in either this or the other TPS sub-families represented in the *A. paniculata* genome.

Oxidational decoration of the diterpene scaffold by *A. paniculata* cytochrome P450 and 2-oxoglutarate-dependent dioxygenase

From common backbones, diterpene scaffolds are often further modified to diterpenoids, prototypically by cytochrome P450 monooxygenases (CYPs), although 2-oxoglutarate-dependent dioxygenases (2OGDs) appear to play a role in certain cases as well (Swaminathan *et al.*, 2009; Q., Wang *et al.*, 2012; Xu and Song, 2017; Kakizaki *et al.*, 2017). Thus, while biosynthesis of andrographolide and neoandrographolide is believed to rely on CYPs (Garg *et al.*, 2015; Cherukupalli *et al.*, 2016), 2OGDs may also play a role. In the

A. paniculata genome, 278 CYP genes were found by automated matching to the relevant Hidden Markov (HMM) model (PF00067), with subsequent manual assignment to the appropriate CYP families (i.e., by Prof. David Nelson, Univ. Tenn.). This is similar to the number found in other angiosperms (Nelson and Werck-Reichhart, 2011). Members of the CYP71 and CYP76 families have been shown to be involved in labdane-related diterpenoid biosynthesis in other Lamiales species (Banerjee and Hamberger, 2018). Genes for a total of 43 CYP71 and 14 CYP76 family members were found in the *A. paniculata* genome (**Supplementary Table 14)**. Expression analysis indicated that transcripts for 18 CYP71 and 6 CYP76 family members accumulate after MeJA treatment ($P < 0.05$) (**Supplementary Table 13**), suggesting that some of these may play a role in biosynthesis of andrographolide and related diterpenoids. A total of 112 putative 2OGDs were found in the *A. paniculata* genome by automated matching to the 2OG-FeII_Oxy DTT domain (PF03171). This is similar to the number of 2OGDs found in other plants, such as *Oryza sativa* (114) and *A. thaliana* (130). The 2OGDs have been phylogenetically divided into three functionally distinct classes (Xu and Song, 2017), and *A. paniculata* has members of all three – i.e., DOXA (4), DOXB (21), and DOXC (90) (**Supplementary Table 14**). DOXC class members were further clustered into twelve families, named based on known function – i.e., AOP (6), GA20ox (5), GA3ox (1), GA2ox (10), DAO (4), F3H (3), FLS/ANS (3), CODM/NCS (16), ACO (9), D4H/GSLOH/BX6 (18), H6H (3), S3H (5), and Unknown (7) (**Supplementary Fig. 7**). Expression analysis indicated that transcripts for 17 2OGDs accumulated after MeJA treatment ($P < 0.05$), suggesting that these also might be involved in biosynthesis of andrographolide and related diterpenoids (**Supplementary Table 14**).

Putative diterpenoid biosynthestic gene clusters

With the rapidly growing number of available plant genomes, it has become evident that these often contain gene clusters that encode, at least partially, biosynthetic pathways for specialized metabolites (Nuetzmann and Osbourn, 2015). To determine if *A. paniculata* contains any such clusters for diterpenoid biosynthesis, the genome was assessed as to whether other biosynthetic genes are found near those for the characterized ApCPSs or ApKSLs. Intriguingly, adjacent to *ApCPS3* are two encoding CYP71 family members, while on a separate contig three genes encoding CYP714 family members are linked to *ApKSL1* (**Supplementary Fig. 8**). In addition, *ApCPS4* and *ApCPS5* are found together with genes encoding four CYP76 family members on yet another contig. It can then be hypothesized that these CYPs may be involved in further elaboration of the initial hydrocarbon scaffolds produced by the nearby (co-clustered) CPS(s) or KSL.

UDP-dependent glycosyltransferases in *A. paniculata* genome

Following sequential oxidation by CYP450 and 2OGD, glycosylation by UDP-dependent glycosyltransferases (UGT) is often observed in secondary metabolism. The added glycan moiety confers pharmacological bioactivity, reduced toxicity and increased solubility (Vogt and Jones, 2000; Jones and Vogt, 2001; Lorenc-Kukuła *et al.*, 2004). One of the major bioactive constituents of *A. paniculata*, neoandrographolide, is such a glycosylated diterpenoid lactone. In this study, we used the 44 amino acids

in the PSPG motifs and full-length amino acid sequence of AtUGT71C5 (*A. thaliana*), MtUGT73K1 (*Medicago truncatula*), SgUGT74AC1 (*Siraitia grosvenorii*), SrUGT76G1 (*Stevia rebaudiana*), SrUGT85C2 (*S. rebaudiana*) and AtUGT88A1 (*A. thaliana*) to probe the *A. paniculata* sequence information. A total of 120 putative UGT genes were identified including 99 genes encoding putative full-length UGTs (i.e, that are more than 250 amino acids in length) **(Supplementary Table 15)**. While this is less than the number of characterized *UGT* genes in *A. thaliana* (120), *Medicago* truncatula (187), *Cypripedium* arietinum (125), *Glycine max* (242), *Gossypium hirsutum* (196) and *Lotus japonicus* (188) (Yonekura-Sakakibara and Hanada, 2011; Huang *et al.*, 2015; Yin *et al.*, 2017), it may reflect less glycoslation in this plant species or the incomplete nature of the draft genome assembly. The full-length *A. paniculata* UGT genes were named based on the accepted naming convention for signature PSPG motifs (http://prime.vetmed.wsu.edu/resources/udp-glucuronsyltransferase-homepage) (Mackenzie *et al.*, 2005). A phylogenetic tree constructed from the 120 screened *A. paniculata UGT* proteins as well as all 120 UGT proteins from *A. thaliana* revealed that the *ApUGT* genes clustered into 22 families. Using the classification scheme employed for *A. thaliana* (Ross *et al.*, 2001), these ApUGTs were clustered into 13 groups (A–M) **(Supplementary Fig. 9).**

The metabolic and transcriptomic analyses of the response of *A. paniculata* seedlings to MeJA was used to highlight ApUGTs that might produce neoandrographolide, which is glucosylated andrograpinin. Similar to the accumulation of the other diterpenoid lactones, neoandrographolide content was significantly (4.8-fold) increased within 24h compared with controls **(Fig. 5A)**. Based on previous reports of UGTs involved in terpenoid biosynthesis (Richman et al., 2005; Poppenberger et al., 2005; Sayama et al., 2012), it was hypothesized that neoandrographolide would be produced by a UGT from the UGT71, UGT73, UGT76, UGT85, or UGT88 families. Accordingly, we focused on the 29 ApUGTs from these families, and found that mRNA levels were significantly elevated (>2-fold) by MeJA treatment for a number of these. Namely, CXN00023829 (82.8-fold), CXN00009930 (7.5-fold), CXN00012854 (25.3-fold), CXN00006409 (188.5-fold), CXN00006414 (5.5-fold), CXN00009309 (7.4-fold), CXN00003963 (7.1-fold), CXN00013979 (4.1-fold). In addition, seven genes were found to be highly expresed in leaves. Namely, CXN00004677, CXN00012856, CXN00003107, CXN00000415, CXN00000414, CXN00017140 and CXN00012855. To functionally investigate the ability of these to produce neoandrographolide, nine of these genes were successfully cloned (CXN00006414, CXN00000414, CXN00000415, CXN00003963, CXN00003107, CXN00013979, CXN00012856, CXN00017140 and CXN00004677), which were named UGT73AU1, UGT76T1, UGT76T2, UGT85A51, UGT85A52, UGT85E6, UGT88A14, UGT88D10 and UGT88L1, respectively. These were then expressed in *E. coli*, and the recombinant proteins purified and evaluated with enzymatic assays **(Supplementary Fig. 10)**. Sequence alignment of these nine ApUGTs with the UGTs from *Stevia rebaudiana* that play a role in glycosylating a similar labdane-related diterpenoid (Brandle and Telmer, 2007; Richman *et al.*, 2005), revealed a conserved domain containing the PSPG motif near their C-terminal domain **(Fig. 5B; Supplementary Fig. 10)**. The last glutamine (Q) residue within this PSPG motif is thought to confer specificity for UDP-glucose as the sugar donor for glycosylation (Kubo *et al.*, 2004). Notably, three ApUGTs possess this Q, suggesting they may all use UDP-glucose as a sugar donor. Two sugar donors (UDP-glucose and UDP-glucuronic acid) and three andrographolide-like aglycones (andrographolide, andrograpanin and 14-deoxy-11,12-didehydroandrographolide) were tested as substrates. We found that of the UGTs tested,

only recombinant UGT73AU1 exhibited catalytic activity, specifically with andrograpanin and 14-Deoxy-11,12-didehydroandrographolide and UDP-glucose as the sugar donor **(Fig. 5C, and Supplementary Fig. 11)**. No activity was detected for the remaining eight recombinant UGT proteins with any of the tested aglycone substrates, regardless of sugar donor. The enzymatic products analyzed via UPLC showed new products were produced with andrograpanin and 14-deoxy-11,12-didehydroandrographolide **(Supplemental Fig. 11)** as compared to corresponding controls. UPLC-Q-TOF MS analysis revealed that these products contained fragments with *m/z* of 162 and were characterized by the loss of one glucose. This loss yielded corresponding aglycones with each substrate **(Fig. 5D and Supplementary Fig. 11)**, indicating they were andrographolide-like monoglucosides. When compared to reference standards, it was verified that these compounds were neoandrographolide and 14-deoxy-11,12-didehydroandrographoside, derived from andrograpanin and 14-deoxy-11,12-didehydroandrographolide, respectively. UGT73AU1 exhibited higher enzymatic activity with andrograpanin (1 nkat/mg) than 14-deoxy-11,12-didehydroandrographolide (0.35 nkat/mg). Given its observed activity, UGT73AU1 seems to discriminate against the 14-hydroxyl found in andrographolide, which does not serve as a substrate, as this is not found in the andrograpanin and 14-deoxy-11,12-didehydroandrographolide that it does react with.

Putative diterpenoid-associated regulatory genes after MeJA induction

A promising approach to increasing plant secondary metabolite production is the utilization of transcription factors (TFs) that stimulate gene expression of the enzymes that comprise the relevant biosynthetic pathways. Several types of TFs that participate in sesquiterpenes, diterpenoid, triterpenoid and monoterpenoid alkaloid biosynthesis have been characterized, belonging to the families of AP2/ERF (APETALA2/Ethylene-Response Factors), bHLH (basic Helix-LoopHelix), and WRKY (Yamamura *et al.*, 2015; Zhang *et al.*, 2011; Yamada *et al.*, 2011; Schweizer *et al.*, 2013; Van Moerkercke *et al.*, 2015; Schluttenhofer and Yuan, 2015; Rushton *et al.*, 2010; Yu *et al.*, 2012; Lu *et al.*, 2013; Shen *et al.*, 2016; Zhou *et al.*, 2016) A total of 1,489 genes in *A. paniculata* are predicted to encode transcription factors (TFs), including 115 members of the bHLH and 67 members of the WRKY families (**Supplementary Table 16**). Here we found that labdane-diterpenoid biosynthesis from *A. paniculata* responds strongly to MeJA elicitation, which is known to induce TFs involved in such regulation of a variety of secondary metabolite biosynthesis (van der Fits and Memelink, 2000; Van der Fits and Memelink, 2001; Zhang *et al.*, 2011; De Geyter *et al.*, 2012). To identify putative regulators of the andrographolide pathway, 94 candidate transcriptional factors were selected by mining the RNA-seq data for TFs whose transcript levels were significantly increased following elicitation with MeJA ($P < 0.05$; Supplementary Table 15), indicating a potential role in regulation of such labdane-diterpenoid biosynthesis. Functional characterization of these TFs using transient system such as virus induced silencing (VIGS) and over-expression, in combination with metabolite analysis, will be employed in the future.

In summary, extensive utilization of the whole plant of *A. paniculata* as an anti-inflammatory drug for the treatment of fever, cold, laryngitis, diarrhea, and inflammation in India and China has led to a broad range of phytochemical/pharmacological studies that have reported the discovery of anti-inflammatory activity for a diverse array of diterpenoid lactones, particularly andrographolide and neoandrographolide. With advent of next-generation sequencing techniques, –omics analyses of non-model plants are now feasible. Here, the *A. paniculata* genome is reported, providing a foundation for cultivar breeding. Along with the tissue-specific and MeJA-induced transcriptomes also reported here, this further provides a rich dataset for mining candidate genes involved in production and regulation of the *A. paniculata* bioactive diterpenoid lactone natural products. For example, the CYP and 2OGD oxygenase superfamilies in *A. paniculata* were annotated, generating a set of tailoring enzymes for future investigation of diterpenoid lactone biosynthesis. In addition, the identification of putative transcription factors on a genome wide-scale is expected to facilitate better understanding of the underlying regulation of such metabolism. The utility of the generated sequence data was more directly demonstrated by functional characterization of *A. paniculata* diterpene synthases, revealing the capacity for production of a variety of labdane-related diterpene backbones. Moreover, a UGT was found that catalyzes glucosylation of andrograpanin to the bioactive neoandrographolide. Accordingly, the data reported here is expected provide the basis for further insights into production of the bioactive diterpenoid lactone constituents of *A. paniculata*.

Methods

Plant materials for sequencing

A. paniculata plants were cultivated in greenhouse at institute of Chinese Materia Medica, China. Genomic DNA was extracted from leaves of one *A. paniculata*, using the plant DNA extraction protocol (Tiangen co. Ltd. Beijing China). For RNA-seq, RNA samples were prepared from root, vegetative stem, young leaf, open flower, mature fruit and cotyledons of seedlings sprayed with 50mM MeJA for 0, 24- and 48-hours using RNeasy Plant Mini Kit (Qiagen Germany). The quality and quantity of the isolated DNA and RNA were checked by electrophoresis on a 0.8% agarose gel and Epoch (BioTek Instruments, USA).

Estimation of the genome size

Both flow cytometry and *k*-mer analysis were utilized for estimating the size of the *A. paniculata* genome prior to whole genome sequencing. Flow cytometry analysis for the measurement of nuclear DNA content was performed using a Partec CA II (Partec, Munster, Germany).

Genome sequencing and assembly

PacBio SMRTbell libraries (20 kb inserts) were prepared with the standard PacBio library preparation protocols, and the sequencing was conducted on a PacBio RS II (Pacific Biosciences, USA) system using P6-C4 chemistry (Novogene Corporation, Ltd Beijing, China). This generated 1.2M SMRT long reads with a total length of 11.8 Gb. The longest read has a length of 78,939 bp, while the mean length of all reads is 9,326 bp and the median length is 9,024 bp. More than 93% of the reads have lengths longer than 1 Kb and more than 44% have lengths longer than 10 Kb (Supplementary table 3). We used Canu v1.5 (Koren *et al.*, 2017) to assemble these SMRT long reads with the following options: 'genomeSize=280m batMemory=256g'.

Hi-C assistant contig clustering

The Hi-C library was prepared by Annoroad Genomics (Beijing, China) following the standard procedure (Lieberman-Aiden *et al.*, 2009). The Hi-C sequencing data were aligned to the assembled contigs by BWAmem, and then the contigs were clustered onto chromosomes with LACHESIS (http://shendurelab.github.io/LACHESIS/).

Gene prediction and annotation

We employed three methods to predict the *A. paniculata* genes: 1) a homology-based method, 2) a de novo method and 3) an EST/transcript-based method. MAKER software was used to predict genes in the assembled genome for the homology-based approach (Cantarel *et al.*, 2008). Prior to de novo gene prediction, DNA and protein related repeat elements were masked using RepeatMaker with the Repbase (Cantarel *et al.*, 2008) and RepeatRunner databases (Tarailo-Graovac and Chen, 2009), respectively. Gene prediction and annotation by ab initio gene prediction utilized RNA and protein evidenced alignments with Augustus software (http://www.yandell-lab.org/software/repeatrunner.html). To validate and complete the gene predictions, transcriptomes from root, shoot, leaf, flower and fruit material were assembled using Trinity (Haas *et al.*, 2013), with default parameters, which were aligned with the assembled genome using Blastn (Camacho *et al.*, 2009). For annotation of protein-coding genes, the nucleotide sequences of high-confidence genes were searched against NCBI, KEGG, Pfam (Bateman, 2004) and Swissport databases with a minimal e-value of 1e-5. BUSCO was then used to assess completeness of the final genome assembly (Waterhouse et al., 2018). The localizations of deduced proteins were predicted using the TargetP 1.1 server (http://www.cbs.dtu.dk/services/TargetP/) (Emanuelsson et al., 2007).

TEs and repetitive DNA

To predict the TEs in the *A. paniculata* genome, we employed a combined methodology, which incorporated *de novo* and homology-based methods. First, a TE library was constructed using RepeatModeler (Tarailo-Graovac and Chen, 2009), and then RepeatMasker used to align the assembled

genome to perform *de novo* prediction and find known TEs using a TE library composed from the Repbase database.

Phylogenetic tree and evolutionary analysis

Phylogenetic construction from the genomes of *A. paniculata* with *A. thaliana*, *G. max*, *M. guttatus*, *O. sativa*, *Populus trichocarpa*, *S. lycopersicum*, *S. tuberosum*, *V. vinifera*, *Zea mays*, *S. indicum* and *U. gibba* was carried out using MrBayes (V3.1.2) software (Ronquist and Huelsenbeck, 2003) based on the HKY85 model (Hasegawa *et al.*, 1985) selected by Modeltest v3.7 (Posada and Crandall, 1998), in which Akaike Information Criterion (AIC) was use to select the best model. The robustness of the retrieved tree topology was also assessed by running the Maximum likelihood method implemented in RAxML v8.2.10 (Stamatakis, 2014)**(Supplementary Fig. 12)**. The divergence time of selected species was analyzed using the program MCMCTree of the PAML package (V4.4) (Yang, 2007). Fossil divergence time points for the *S. lycopersicum/S. tuberosum* split (7.2~7.4 mya) (Sato *et al.*, 2012), *O. sativa/ Z. mays* split (> 20mya) (Paterson *et al.*, 2009; Paterson *et al.*, 2004) and *O. sativa/ V. vinifera* split (130~240 mya) (Jaillon *et al.*, 2007) were used to calibrate the tree. *Ks* analysis was conducted by firstly using MCscanX to obtain genomic collinear blocks (Wang *et al.*, 2012), then program YN00 from the PAML package was used to calculate *Ks* values of gene pairs contained in collinear blocks. In order to get the gene families from the selected 14 species, OrthoMCL (V1.4) was used for gene clustering, setting the main inflation value to 1.5 and with other default parameters (Li *et al.*, 2003). Then CAFÉ software (V2.1) was used for contraction and expansion analysis of these gene families (De Bie *et al.*, 2006). For phylogenetic reconstruction of the diterpene synthase, 2-oxoglutarate-dependent dioxygenase and UDP-glycosyl transferase families, neighbor-joining phylogenetic analyses with 1000 bootstrap repetitions were performed using MEGA version 5.02 beta (Kumar *et al.*, 2016).

Metabolite detection

UHPLC/MS/MS was used to quantify the levels of nine diterpenoid lactones in *A. paniculata* seedlings after 50 mM MeJA treatment. Fresh samples were powdered in liquid nitrogen and 100 mg extracted with 15 mL of methanol in an ultrasonic bath at 25 ℃ for 30 min. Resulting sample solutions, as well as nine standard compounds (andrographolide, andropanolide, 14-deoxyandrographolide, neoandrographolide, andrograpanin, andropanoside, 14-deoxy-11-hydroxyandrographolide, 14-deoxy-17-hydroxyandrographolide and 14-Deoxy-11,12-dideroxyandrographoside) from BioBioPha Co., Ltd. (Kunming China), were filtered through a 0.22-μm membrane, and 2-μL aliquots injected for analysis. A 1290 series UHPLC was coupled with a 6470 triple quadrupole mass spectrometer via an AJS-ESI interface (Agilent Technologies, Waldbronn, Germany). Samples were separated over an Agilent Eclipse Plus C18 column (RRHD 1.8μm, 2.1×50mm). The A and B mobile phases were acetonitrile and water solutions containing 0.1% formic acid, respectively. The analytes were eluted using a linear gradient program: 0~2 min, 6→25% B; 2~6 min, 25→30% B; 6~7 min, 30→80% B; 6~10 min, 80→100% B; 10~11 min, 100% B. The flow rate was 0.30 mL/min and column temperature was 30 ℃. The mass

spectrometer was operated in positive ion mode, with sheath gas temperature at 250 °C, gas flow at 11.0 L/min, and nebulizer gas at 40 psi. The capillary voltage was set at 4000 V, nozzle voltage to 500 V, and delta EMV to 200 V. Metabolites were detected in multiple reaction monitoring (MRM) mode, where two precursor-product ion MRM transitions were selected for each compound (one for quantitation and the other for qualification), as shown in the Supporting Information. Data was acquired and analyzed using MassHunter (version B.07.00) to quantify all nine metabolites for which standards were available.

Isolation of five *ApCPS/KSL*s and nine *ApUGT*s from *A. paniculata*

Using plant RNA extraction protocols (Tiangen co. Ltd. Beijing China), total RNA was extracted from the leaf of *A. paniculata* for cDNA synthesis. First-strand cDNA was synthesized using the PrimeScript First-Strand cDNA Synthesis Kit and oligo(dT) primer (Takara, Japan). Primers were designed for three *ApCPS*s, two *ApKSL*s and nine *ApUGT*s (from different UGT families) according to the *A. paniculata* genome sequence and used to clone these full-length genes which were inserted into pEASY blunt vector (TransGen Biotech, Beijing, China) for Sanger sequencing using an ABI3730 DNA Sequencer (Applied Biosystems, Foster City, CA, USA) (**Supplementary Table 17**).

UGT Gene expression analysis

Total RNA was reverse transcribed into cDNA using the TransScript II One-Step gDNA Removal and cDNA Synthesis SuperMix (TransGen Biotech, Beijing, China), according to the manufacturers protocol. Ten-fold diluted cDNA was used as template for subsequent qRT-PCR analysis using TransStart Green qPCR SuperMix (TransGen Biotech, Beijing, China) on Rotor-Gene Q MDx (QIAGEN Co., Hilden, Germany), with primers sequences that can be found in **Supplementary Table 17**. These PCR reactions were performed using the following cycling parameters: 95 °C for 7 min (enzyme activation), 35 cycles of 95 °C for 15 s, 60 °C for 30 s, and 72 °C for 30 s, followed by a melting curve cycle from 60 °C to 90 °C. The results were normalized against actin as a reference gene. Relative transcript level was calculated as the mean of three technical replicates of three biological replicates.

Functional Characterization of *ApCPS/KSL* genes

The *ApCPS1* and *ApCPS3* genes were truncated to remove the N-terminal plastid targeting sequence for expression of pseudo-mature enzymes in *E. coli*. These constructs were generated by PCR, and first cloned in pENTR-SD-dTOPO (Invitrogen, Carlsbad, CA, USA), with the corresponding insert verified by complete gene sequencing. Each gene was then individually sub-cloned by directional recombination into a previously described pGG-DEST vector (Cyr et al., 2007), creating pGG-DEST::ApCPS1 & 3 expression constructs. These were used to examine product outcome, first by expression alone, and then co-expression with compatible pDEST14 based AS or KS constructs to examine stereospecific product outcome. Similarly, ApKSL1 & 2 were truncated to remove the N-terminal plastid targeting sequence for expression of pseudo-mature enzymes in *E. coli*. These constructs were generated by PCR, and first cloned in

pENTR-SD-dTOPO (Invitrogen, Carlsbad, CA, USA), with the corresponding insert verified by complete gene sequencing. Each gene was then individually sub-cloned by directional recombination into pDEST14, creating pDEST14::ApKSL1 & 2 expression constructs. These were used to examine product outcome by co-expression with previously described compatible pGGeC, pGGsC and pGGnC vectors, which lead to production of *ent*-, *syn*- or normal CPP, respectively, as previously described (Cyr *et al.*, 2007).

Expression and purification of recombinant UGT proteins in *E. coli*.

The UGTs were sub-cloned to construct pMAL-UGT expression vectors, which were then transformed into *E. coli* strain Novablue competent cells. To induce protein expression, 0.3 mM of isopropyl β-D-thiogalactoside (IPTG) was added when the OD_{600} value of cell culture (grown at 37 ℃) reached 0.5. After 24 h incubation with shaking at 16 ℃, the cells were harvested by centrifugation at 4 ℃ and then stored at -80 ℃ until purification. The MBP-fusion proteins were purified using protocols for the pMAL Protein Fusion and Purification System (New England BioLabs). The recombinant UGT proteins (5 μg -10 μg) were incubated for 1 hour at 37 ℃ in a final volume of 50 μL comprised of 10 mM dithiothreitol （DTT）, 20 mM Tris-HCl (pH 7.0), 0.5 mM substrates and 2 mM UDP-glucose or UDP-glucuronic acid. Reactions were stopped by the addition of methanol and centrifuged at 14,000 rpm for 10 min, followed by analysis via UPLC. To investigate the enzymatic specificity of the recombinant UGT73AU1, purified enzyme (5-10 μg) were incubated for 30 minutes at 37 ℃ in 50 μL reaction mixtures comprising 10 mM DTT, 20 mM Tris-HCl (pH 7.0), 0.5 mM substrates and 2 mM UDP-glucose. Reactions were terminated by adding methanol, centrifuged at 14,000 rpm for 10 min, and also analyzed via UPLC. The enzymatic products were further identified by Q-TOF-MS, as described below. Acquity ultra performance liquid chromatography (UPLC, Agilent 1290 Infinity II) consisting of an autosampler and a binary pump was used for analysis. Specifically, the compounds were separated over an EclipsePlusC18 RRHD (1.8μm, 2.1×50 mm i.d.; Agilent) analytical column at a temperature of 30 ℃, with a sample injection volume of 2 μL. A gradient elution was achieved using two solvents: 0.1% formic acid in water (A) or acetonitrile (B), at a flow rate of 0.3 mL/min. The gradient program consisted of: 0-2min, 74% A; 2-4min, 68% A; 4-12min, 62% A; 12-20min, 55% A; 20-22min, 95% B; 22-24min, 95% A for balancing; with a return to initial conditions over 1 min. The detected wavelength was 203 nm. The UPLC system used was interfaced with a 6545 Q-TOF LC/MS (Agilent), equipped with an electrospray (Turbo V TM) ion source. The MS was used in positive-ion mode with the following conditions: dual AJS ESI (Seg): gas temp, 325 ℃; drying gas, 5 L/min; nebulizer, 35 psig; sheath gas temp, 350 ℃; sheath gas flow, 11 L/min. dual AJS ESI (Expt): V_{cap}, 3500V; nozzle voltage (Expt), 500V. MS TOF (Expt): fragmentor, 130V; skimmer, 65V; Oct 1 RF V_{pp}, 750V; and collected signal *m/z*: 100-1000.

Data submission

ACCESSION NUMBERS The clean reads are deposited in Sequence Read Archive (SRA) under SRP143459.

AUTHORS' CONTRIBUTIONS

W. S., C. S., R. P. and S. L. C. designed experiments. W. S. isolated genomic DNA and RNA from different tissues and MeJA treated seedling. C. S. performed assemblies of the Illumina data and evolutionary analysis. L. L. performed assemblies for PacBiosystems sequence data. W. S., M. M. X. and Q. G. Y. cloned and characterized gene function. W. S., C. X. and S. C. performed LC mass spectrometry assays. W. S., L. L., Q. G. Y. and R. J. P. wrote the manuscript with input from the other co-authors. X. L. Z., N. X. and C. H. J. were responsible for plant germplasm collection. All authors read and approved the final manuscript.

ACKNOWLEDGMENTS

This work was supported by National Natural Science Foundation of China (81703647), the US National Institutes of Health (GM076324) and National Postdoctoral Program for Innovative Talents Fund (BX201600155).

The authors declare no conflicts of interest.

SHORT SUPPORTING INFORMATION LEGENDS

Supplementary Figures

Figure S1 Evaluation of the genome size of *A. paniculata* by flow cytometry.

Figure S2 Evaluation of the genome size of *A. paniculata* by 17-*mer* analyses.

Figure S3 Genome wide Hi-C heatmap.

Figure S4 *Ks* distributions of syntenic paralogs and orthologs from *A. paniculata, S. indicum, V. vinfera* and *S. lycopersicum.*

Figure S5 Four sequence comparison of the *A. paniculata* copalyl diphosphate synthase (CPS) enzymatic family with two CPS genes from *Marrubium vulgare*.

Figure S6 Two sequence comparison of the *A. paniculata* kaurene synthase-like (KSL-like) enzymatic family with three previously characterized KSL enzymes from *Oryza sativa*.

Figure S7 Analysis of the phylogenetic relationships of 2OGD gene members in *A. paniculata.*

Figure S8 Physical clustering of diterpenoid pathway gene in *A. paniculata*.

Figure S9 NJ tree of the UGT family shows 13 distinct groups (A–M) based on aligned protein sequences.

Figure S10 Multiple sequence alignment of PSPG motifs of ApUGTs and three purified recombinant UGT proteins on denaturing PAGE.

Figure S11 Characterization of rApUGT73AU1 activity with 14-Deoxy-11,12-didehydroandrographolide.

Figure S12 Phylogeny of *A. paniculata* and eleven other species estimated by the Maximum likelihood method.

Supplementary Tables

Table S1 Sequencing summary of Pacbio SMRT library.

Table S2 Summary of some plant genomes published recently.

Table S3 Estimation of *A. paniculata* genome by RNA-seq and BUSCO results

Table S4 Contigs anchored to pseudo molecules.

Table S5 Summary of gene annotation.

Table S6 Summary of gene families.

Table S7 Functional enrichment analysis of the genes specific to *A. paniculata* plant using InterPro database.

Table S8 Functional enrichment analysis of the genes belonging to families specifically expanded in the *A. paniculata* genome

Table S9 TE categories and contents in *A. paniculata* genome.

Table S10 MEP, MVA, IPPI and GGPPS-like genes in *A. paniculata* genome.

Table S11 FPKM expression levels of MEP, MVA, IPPI and GGPPS-like genes in *A. paniculata* genome.

Table S12 The CPS and KSL protein sequences from *A. paniculata* and other species for phylogenetic reconstruction this study.

Table S13 FPKM expression levels of P450 genes from CYP71 and 76 families.

Table S14 2OGD genes in *A. paniculata* genome and their expression pattern.

Table S15 UGT genes expression in different tissues and seedlings treated with MeJA.

Table S16 List of transcription factor genes predicted in the *A. paniculata.*

Table S17 Characterization of ApCPS, KSL and UGT. This spreadsheet lists the gene names, their corresponding IDs and genbank numbers, as well as the primers used for cloning of every individual sequence characterized in the paper.

References

Ajaya Kumar, R., Sridevi, K., Vijaya Kumar, N., Nanduri, S. and Rajagopal, S. (2004) Anticancer and immunostimulatory compounds from Andrographis paniculata. *J. Ethnopharmacol.*, **92**, 291–295.

Amroyan, E., Gabrielian, E., Panossian, A., Wikman, G. and Wagner, H. (1999) Inhibitory effect of andrographolide from Andrographis paniculata on PAF-induced platelet aggregation. *Phytomedicine*, **6**, 27–31.

Anju, D., Jugnu, G., Kavita, S., Arun, N. and Sandeep, D. (2012) a Review on Medicinal Prospectives of Andrographis Paniculata Nees. *J. Pharm. Sci. Innov.*, **1**, 1–4.

Avani, G. and Rao, M. V. (2008) In vitro cytogenetic effects of Andrographis paniculata (kalmegh) on arsenic. *Phytomedicine*, **15**, 221–225.

Banerjee, A. and Hamberger, B. (2018) P450s controlling metabolic bifurcations in plant terpene specialized metabolism. *Phytochem. Rev.*, **17**, 81–111.

Bateman, A. (2004) The Pfam protein families database. *Nucleic Acids Res.*

Benoy, G.K., Animesh, D.K., Aninda, M., Priyanka, D.K. and Sandip, H. (2012) An overview on andrographis paniculata (burm. F.) Nees. *Int. J. Res. Ayurveda Pharm.*, **3**, 752–760.

Bie, T. De, Cristianini, N., Demuth, J.P. and Hahn, M.W. (2006) CAFE: a computational tool for the study of gene family evolution. *Bioinformatics*, **22**, 1269–71.

Brandle, J.E. and Telmer, P.G. (2007) Steviol glycoside biosynthesis. *Phytochemistry*.

Camacho, C., Coulouris, G., Avagyan, V., Ma, N., Papadopoulos, J., Bealer, K. and Madden, T.L. (2009) BLAST+: architecture and applications. *BMC Bioinformatics*, **10**, 421.

Cantarel, B.L., Korf, I., Robb, S.M.C., Parra, G., Ross, E., Moore, B., Holt, C., Alvarado, A.S. and Yandell, M. (2008) MAKER: An easy-to-use annotation pipeline designed for emerging model organism genomes. *Genome Res.*, **18**, 188–196.

Chandrasekaran, C. V., Gupta, A. and Agarwal, A. (2010) Effect of an extract of Andrographis paniculata leaves on inflammatory and allergic mediators in vitro. *J. Ethnopharmacol.*, **129**, 203–207.

Chao, W.-W. and Lin, B.-F. (2010) Isolation and identification of bioactive compounds in Andrographis paniculata (Chuanxinlian). *Chin. Med.*, **5**, 17.

Chen, F., Tholl, D., Bohlmann, J. and Pichersky, E. (2011) The family of terpene synthases in plants: A mid-size family of genes for specialized metabolism that is highly diversified throughout the kingdom. *Plant J.*

Chen, H., Jones, A.D. and Howe, G.A. (2006) Constitutive activation of the jasmonate signaling pathway enhances the production of secondary metabolites in tomato. *FEBS Lett.*, **580**, 2540–2546.

Chen, L.R., Chen, Y.J., Lee, C.Y. and Lin, T.Y. (2007) MeJA-induced transcriptional changes in adventitious roots of Bupleurum kaoi. *Plant Sci.*, **173**, 12–24.

Cherukupalli, N., Divate, M., Mittapelli, S.R., Khareedu, V.R. and Vudem, D.R. (2016) De novo Assembly of Leaf Transcriptome in the Medicinal Plant Andrographis paniculata. *Front. Plant Sci.*

Criswell, J., Potter, K., Shephard, F., Beale, M.H. and Peters, R.J. (2012) A single residue change leads to a hydroxylated product from the class II diterpene cyclization catalyzed by abietadiene synthase. *Org. Lett.*, **14**, 5828–5831.

Cyr, A., Wilderman, P.R., Determan, M. and Peters, R.J. (2007) A modular approach for facile biosynthesis of labdane-related diterpenes. *J. Am. Chem. Soc.*, **129**, 6684–6685.

Emanuelsson, O., Brunak, S., Heijne, G. von and Nielsen, H. (2007) Locating proteins in the cell using TargetP, SignalP and related tools. *Nat. Protoc.*

Fits, L. van der and Memelink, J. (2000) ORCA3, a jasmonate-responsive transcriptional regulator of plant primary and secondary metabolism. *Science*, **289**, 295–297.

Fits, L. Van der and Memelink, J. (2001) The jasmonate-inducible AP2/ERF-domain transcription factor ORCA3 activates gene expression via interaction with a jasmonate-responsive promoter element. *Plant J.*, **25**, 43–53.

Garg, A., Agrawal, L., Misra, R.C., Sharma, S. and Ghosh, S. (2015) Andrographis paniculata transcriptome provides molecular insights into tissue-specific accumulation of medicinal diterpenes. *BMC Genomics*, **16**, 659.

Geyter, N. De, Gholami, A., Goormachtig, S. and Goossens, A. (2012) Transcriptional machineries in jasmonate-elicited plant secondary metabolism. *Trends Plant Sci.*, **17**, 349–359.

Goel, A., Kunnumakkara, A.B. and Aggarwal, B.B. (2008) Curcumin as "Curecumin": From kitchen to clinic. *Biochem. Pharmacol.*, **75**, 787–809.

Haas, B.J., Papanicolaou, A., Yassour, M., et al. (2013) De novo transcript sequence reconstruction from RNA-seq using the Trinity platform for reference generation and analysis. *Nat. Protoc.*, **8**, 1494–1512.

Hansen, N.L., Heskes, A.M., Hamberger, B., Olsen, C.E., Hallström, B.M., Andersen-Ranberg, J. and Hamberger, B. (2016) The terpene synthase gene family in Tripterygium wilfordii harbors a labdane-type diterpene synthase among the monoterpene synthase TPS-b subfamily. *Plant J.*

Hasegawa, M., Kishino, H. and Yano, T. (1985) Dating the human-ape split by a molecular clock of mitochondrial DNA. *Evolution (N. Y).*

Huang, J., Pang, C., Fan, S., et al. (2015) Genome-wide analysis of the family 1 glycosyltransferases in cotton. *Mol. Genet. Genomics*, **290**, 1805–1818.

Inabuy, F., Fischedick, J.T., Lange, I., Hartmann, M., Srividya, N., Parrish, A.N., Xu, M., Peters, R.J. and Lange, B.M. (2017) Biosynthesis of Diterpenoids in Tripterygium Adventitious Root Cultures. *Plant Physiol.*, pp.00659.2017.

Jaillon, O., Aury, J.M., Noel, B., et al. (2007) The grapevine genome sequence suggests ancestral hexaploidization in major angiosperm phyla. *Nature*.

Jian, W.W. and Wu, J.Y. (2005) Nitric oxide is involved in methyl jasmonate-induced defense responses and secondary metabolism activities of Taxus cells. *Plant Cell Physiol.*, **46**, 923–930.

Jones, P. and Vogt, T. (2001) Glycosyltransferases in secondary plant metabolism: Tranquilizers and stimulant controllers. *Planta*, **213**, 164–174.

Kakizaki, T., Kitashiba, H., Zou, Z., Li, F., Fukino, N. and Ohara, T. (2017) A 2-Oxoglutarate-Dependent Dioxygenase Mediates the Biosynthesis of Glucoraphasatin in Radish 1 [OPEN]. , **173**, 1583–1593.

Kamboj, V. (2000) Herbal medicine. *Curr. Sci.*, **78**, 35–39.

Kanehisa, M. and Goto, S. (2000) KEGG : Kyoto Encyclopedia of Genes and Genomes. *Nucleic Acid Res.*

Kim, H.-J., Chen, F., Wang, X. and Rajapakse, N.C. (2006) Effect of methyl jasmonate on secondary metabolites of sweet basil (Ocimum basilicum L.). *J. Agric. Food Chem.*, **54**, 2327–32.

Koren, S., Walenz, B.P., Berlin, K., Miller, J.R., Bergman, N.H. and Phillippy, A.M. (2017) Canu: Scalable and accurate long-read assembly via adaptive κ-mer weighting and repeat separation. *Genome Res.*, **27**, 722–736.

Koteswara Rao, Y., Vimalamma, G., Venkata Rao, C. and Tzeng, Y.M. (2004) Flavonoids and andrographolides from Andrographis paniculata. *Phytochemistry*, **65**, 2317–2321.

Kubo, A., Arai, Y., Nagashima, S. and Yoshikawa, T. (2004) Alteration of sugar donor specificities of plant glycosyltransferases by a single point mutation. *Arch. Biochem. Biophys.*, **429**, 198–203.

Kumar, S., Stecher, G. and Tamura, K. (2016) MEGA7: Molecular Evolutionary Genetics Analysis Version 7.0 for Bigger Datasets. *Mol. Biol. Evol.*, **33**, 1870–1874.

Lange, B.M., Rujan, T., Martin, W. and Croteau, R. (2000) Isoprenoid biosynthesis: The evolution of two ancient and distinct pathways across genomes. *Proc. Natl. Acad. Sci.*

Li, F. and Weng, J. (2017) Demystifying traditional herbal medicine with. *Nat. Publ. Gr.*, **3**, 1–7.

Li, L., Stoeckert, C.J. and Roos, D.S. (2003) OrthoMCL: Identification of ortholog groups for eukaryotic genomes. *Genome Res.*, **13**, 2178–2189.

Lieberman-Aiden, E., Berkum, N.L. Van, Williams, L., et al. (2009) Comprehensive mapping of long-range interactions reveals folding principles of the human genome. *Science (80-.).*, **326**, 289–293.

Lim, J.C.W., Chan, T.K., Ng, D.S., Sagineedu, S.R., Stanslas, J. and Wong, W.F. (2012) Andrographolide and its analogues: Versatile bioactive molecules for combating inflammation and cancer. *Clin. Exp. Pharmacol. Physiol.*, **39**, 300–310.

Lorenc-Kukuła, K., Korobczak, A., Aksamit-Stachurska, A., Kostyń, K., Lukaszewicz, M. and Szopa, J. (2004) Glucosyltransferase: the gene arrangement and enzyme function. *Cell. Mol. Biol. Lett.*, **9**, 935–46.

Lu, X., Zhang, L., Zhang, F., Jiang, W., Shen, Q., Zhang, L., Lv, Z., Wang, G. and Tang, K. (2013) AaORA, a trichome-specific AP2/ERF transcription factor of Artemisia annua, is a positive regulator in the artemisinin biosynthetic pathway and in disease resistance to Botrytis cinerea. *New Phytol.*, **198**, 1191–1202.

Ma, X.C., Gou, Z.P., Wang, C.Y., Yao, J.H., Xin, X.L., Lin, Y. and Liu, K.X. (2010) A new ent-labdane diterpenoid lactone from Andrographis paniculata. *Chinese Chem. Lett.*, **21**, 587–589.

Ma, Y., Yuan, L., Wu, B., Li, X., Chen, S. and Lu, S. (2012) Genome-wide identification and characterization of novel genes involved in terpenoid biosynthesis in Salvia miltiorrhiza. *J. Exp. Bot.*, **63**, 2809–2823.

Mackenzie, P.I., Bock, K.W., Burchell, B., Guillemette, C., Ikushiro, S., Iyanagi, T., Miners, J.O., Owens, I.S.

and Nebert, D.W. (2005) Nomenclature update for the mammalian UDP glycosyltransferase (UGT) gene superfamily. *Pharmacogenet. Genomics*, **15**, 677–685.

Mafu, S., Potter, K.C., Hillwig, M.L., Schulte, S., Criswell, J.D. and Peters, R.J. (2015) Efficient heterocyclisation by (di)terpene synthases. *Chem. Commun.*, **51**, 13485–13487.

Misra, R.C., Garg, A., Roy, S., Chanotiya, C.S., Vasudev, P.G. and Ghosh, S. (2015) Involvement of an ent-copalyl diphosphate synthase in tissue-specific accumulation of specialized diterpenes in Andrographis paniculata. *Plant Sci.*, **240**, 50–64.

Moerkercke, A. Van, Steensma, P., Schweizer, F., et al. (2015) The bHLH transcription factor BIS1 controls the iridoid branch of the monoterpenoid indole alkaloid pathway in Catharanthus roseus. *Proc. Natl. Acad. Sci. U. S. A.*, **112**, 201504951.

Nelson, D. and Werck-Reichhart, D. (2011) A P450-centric view of plant evolution. *Plant J.*

Nuetzmann, H.-W. and Osbourn, A. (2015) Regulation of metabolic gene clusters in Arabidopsis thaliana. *New Phytol.*, **205**, 503–510.

Pal, S. and Shukla, Y. (2003) Herbal medicine: current status and the future. *Asian Pacific J. Cancer Prev.*, **4**, 281–288.

Paterson, A.H., Bowers, J.E., Bruggmann, R., et al. (2009) The Sorghum bicolor genome and the diversification of grasses. *Nature*.

Paterson, A.H., Bowers, J.E. and Chapman, B.A. (2004) Ancient polyploidization predating divergence of the cereals, and its consequences for comparative genomics. *Proc. Natl. Acad. Sci.*

Peters, R.J. (2010) Two rings in them all: the labdane-related diterpenoids. *Nat. Prod. Rep.*, **27**, 1521–1530.

Peters, R.J., Flory, J.E., Jetter, R., Ravn, M.M., Lee, H.J., Coates, R.M. and Croteau, R.B. (2000) Abietadiene synthase from grand fir (Abies grandis): Characterization and mechanism of action of the “pseudomature” recombinant enzyme. *Biochemistry*, **39**, 15592–15602.

Peters, R.J., Ravn, M.M., Coates, R.M. and Croteau, R.B. (2001) Bifunctional abietadiene synthase: Free diffusive transfer of the (+)-copalyl diphosphate intermediate between two distinct active sites. *J. Am. Chem. Soc.*, **123**, 8974–8978.

Pholphana, N., Rangkadilok, N., Saehun, J., Ritruechai, S. and Satayavivad, J. (2013) Changes in the contents of four active diterpenoids at different growth stages in Andrographis paniculata (Burm.f.) Nees (Chuanxinlian). *Chin. Med.*, **8**, 2.

Poppenberger, B., Fujioka, S., Soeno, K., et al. (2005) The UGT73C5 of Arabidopsis thaliana glucosylates brassinosteroids. *Proc Natl Acad Sci U S A*, **102**, 15253–15258.

Posada, D. and Crandall, K.A. (1998) MODELTEST: Testing the model of DNA substitution. *Bioinformatics*.

Potter, K., Criswell, J., Zi, J., Stubbs, A. and Peters, R.J. (2014) Novel product chemistry from mechanistic analysis of ent-copalyl diphosphate synthases from plant hormone biosynthesis. *Angew. Chemie - Int. Ed.*, **53**, 7198–7202.

Prisic, S., Xu, J., Coates, R.M. and Peters, R.J. (2007) Probing the role of the DXDD motif in class II diterpene

cyclases. *ChemBioChem*, **8**, 869–874.

Raskin, I., Ribnicky, D.M., Komarnytsky, S., et al. (2002) Plants and human health in the twenty-first century. *Trends Biotechnol.*, **20**, 522–531.

Reyes, B.A.S., Bautista, N.D., Tanquilut, N.C., et al. (2006) Anti-diabetic potentials of Momordica charantia and Andrographis paniculata and their effects on estrous cyclicity of alloxan-induced diabetic rats. *J. Ethnopharmacol.*, **105**, 196–200.

Richman, A., Swanson, A., Humphrey, T., Chapman, R., McGarvey, B., Pocs, R. and Brandle, J. (2005) Functional genomics uncovers three glucosyltransferases involved in the synthesis of the major sweet glucosides of Stevia rebaudiana. *Plant J.*, **41**, 56–67.

Ronquist, F. and Huelsenbeck, J.P. (2003) MrBayes 3: Bayesian phylogenetic inference under mixed models. *Bioinformatics*, **19**, 1572–1574.

Ross, J., Li, Y., Lim, E. and Bowles, D.J. (2001) Higher plant glycosyltransferases. *Genome Biol.*, **2**, REVIEWS3004.

Roy Upton, R.H. (2015) *Traditional Herbal Medicine, Pharmacognosy, and Pharmacopoeial Standards: A Discussion at the Crossroads*, Elsevier Inc.

Rushton, P.J., Somssich, I.E., Ringler, P. and Shen, Q.J. (2010) WRKY transcription factors. *Trends Plant Sci.*, **15**, 247–258.

Sato, S., Tabata, S., Hirakawa, H., et al. (2012) The tomato genome sequence provides insights into fleshy fruit evolution. *Nature*, **485**, 635–641.

Sayama, T., Ono, E., Takagi, K., et al. (2012) The Sg-1 Glycosyltransferase Locus Regulates Structural Diversity of Triterpenoid Saponins of Soybean. *Plant Cell*, **24**, 2123–2138.

Sc, M. (2014) " ESTABLISHMENT OF HAIRY ROOT FOR ANDROGRAPHOLIDE PRODUCTION IN Andrographis paniculata ."

Schluttenhofer, C. and Yuan, L. (2015) Regulation of Specialized Metabolism by WRKY Transcription Factors. *Plant Physiol.*, **167**, 295–306.

Schweizer, F., Fernández-Calvo, P., Zander, M., et al. (2013) Arabidopsis basic helix-loop-helix transcription factors MYC2, MYC3, and MYC4 regulate glucosinolate biosynthesis, insect performance, and feeding behavior. *Plant Cell*, **25**, 3117–32.

Sheeja, K., Shihab, P.K. and Kuttan, G. (2006) Antioxidant and anti-inflammatory activities of the plant Andrographis paniculata Nees. *Immunopharmacol. Immunotoxicol.*, **28**, 129–140.

Shen, Q., Lu, X., Yan, T., et al. (2016) The jasmonate-responsive AaMYC2 transcription factor positively regulates artemisinin biosynthesis in Artemisia annua. *New Phytol.*, **210**, 1269–1281.

Singha, P.K., Roy, S. and Dey, S. (2003) Antimicrobial activity of Andrographis paniculata. *Fitoterapia*, **74**, 692–694.

Stamatakis, A. (2014) RAxML version 8: A tool for phylogenetic analysis and post-analysis of large phylogenies. *Bioinformatics*.

Subramanian, R., Asmawi, M.Z. and Sadikun, A. (2012) A bitter plant with a sweet future? A comprehensive review of an oriental medicinal plant: Andrographis paniculata. *Phytochem. Rev.*, **11**, 39–75.

Sudhakaran, M. (2012) Botanical pharmacognosy of Andrographis paniculata (Burm. F.) Wall. Ex. Nees. *Pharmacogn. J.*, **4**, 1–10.

Swaminathan, S., Morrone, D., Wang, Q., Fulton, D.B. and Peters, R.J. (2009) CYP76M7 Is an ent-Cassadiene C11 -Hydroxylase Defining a Second Multifunctional Diterpenoid Biosynthetic Gene Cluster in Rice. *Plant Cell*.

Tang, H., Wang, X., Bowers, J.E., Ming, R., Alam, M. and Paterson, A.H. (2008) Unraveling ancient hexaploidy through multiply-aligned angiosperm gene maps. *Genome Res.*

Tarailo-Graovac, M. and Chen, N. (2009) Using RepeatMasker to identify repetitive elements in genomic sequences. *Curr. Protoc. Bioinforma.*

Tomato Genome Consortium (2012) The tomato genome sequence provides insights into fleshy fruit evolution. *Nature*.

Vekemans, D., Proost, S., Vanneste, K., Coenen, H., Viaene, T., Ruelens, P., Maere, S., Peer, Y. Van De and Geuten, K. (2012) Gamma paleohexaploidy in the stem lineage of core eudicots: Significance for MADS-BOX gene and species diversification. *Mol. Biol. Evol.*, **29**, 3793–3806.

Vogt, T. and Jones, P. (2000) Glycosyltransferases in plant natural product synthesis: characterization of a supergene family. *Trends Plant Sci.*, **5**, 380–386.

Vranová, E., Coman, D. and Gruissem, W. (2013) Network analysis of the MVA and MEP pathways for isoprenoid synthesis. *Annu. Rev. Plant Biol.*, **64**, 665–700.

Wang, G.C., Wang, Y., Williams, I.D., Sung, H.H.Y., Zhang, X.Q., Zhang, D.M., Jiang, R.W., Yao, X.S. and Ye, W.C. (2009) Andrographolactone, a unique diterpene from Andrographis paniculata. *Tetrahedron Lett.*, **50**, 4824–4826.

Wang, H., Ma, C., Li, Z., Ma, L., Wang, H., Ye, H., Xu, G. and Liu, B. (2010) Effects of exogenous methyl jasmonate on artemisinin biosynthesis and secondary metabolites in Artemisia annua L. *Ind. Crops Prod.*, **31**, 214–218.

Wang, L., Yu, S., Tong, C., et al. (2014) Genome sequencing of the high oil crop sesame provides insight into oil biosynthesis. *Genome Biol.*, **15**, R39.

Wang, Q., Hillwig, M.L., Wu, Y. and Peters, R.J. (2012) CYP701A8: A Rice ent-Kaurene Oxidase Paralog Diverted to More Specialized Diterpenoid Metabolism. *Plant Physiol.*, **158**, 1418–1425.

Wang, Y., Tang, H., Debarry, J.D., et al. (2012) MCScanX: A toolkit for detection and evolutionary analysis of gene synteny and collinearity. *Nucleic Acids Res.*

Waterhouse, R.M., Seppey, M., Simao, F.A., Manni, M., Ioannidis, P., Klioutchnikov, G., Kriventseva, E. V. and Zdobnov, E.M. (2018) BUSCO applications from quality assessments to gene prediction and phylogenomics. *Mol. Biol. Evol.*

World Health Organization (2002) Flos Caryophylli. *WHO Monogr. Vol. 2*, **2**, 45–52.

Xu, H., Song, J., Luo, H., et al. (2016) Analysis of the Genome Sequence of the Medicinal Plant Salvia miltiorrhiza. *Mol. Plant*.

Xu, Z. and Song, J. (2017) The 2-oxoglutarate-dependent dioxygenase superfamily participates in tanshinone production in Salvia miltiorrhiza. , **68**, 2299–2308.

Yamada, Y., Koyama, T. and Sato, F. (2011) Basic helix-loop-helix transcription factors and regulation of alkaloid biosynthesis. *Plant Signal. Behav.*, **6**, 1627–30.

Yamaguchi, S., Sun, T.P., Kawaide, H. and Kamiya, Y. (1998) The GA2 locus of Arabidopsis thaliana encodes ent-kaurene synthase of gibberellin biosynthesis. *Plant Physiol.*, **116**, 1271–1278.

Yamamura, C., Mizutani, E., Okada, K., et al. (2015) Diterpenoid phytoalexin factor, a bHLH transcription factor, plays a central role in the biosynthesis of diterpenoid phytoalexins in rice. *Plant J.*, **84**, 1100–1113.

Yang, Z. (2007) PAML 4: Phylogenetic analysis by maximum likelihood. *Mol. Biol. Evol.*, **24**, 1586–1591.

Yin, Q., Shen, G., Chang, Z., Tang, Y., Gao, H. and Pang, Y. (2017) Involvement of three putative glucosyltransferases from the UGT72 family in flavonol glucoside/rhamnoside biosynthesis in Lotus japonicus seeds. *J. Exp. Bot.*, **68**, 597–612.

Yonekura-Sakakibara, K. and Hanada, K. (2011) An evolutionary view of functional diversity in family 1 glycosyltransferases. *Plant J.*, **66**, 182–193.

Yu, Z.X., Li, J.X., Yang, C.Q., Hu, W.L., Wang, L.J. and Chen, X.Y. (2012) The jasmonate-responsive AP2/ERF transcription factors AaERF1 and AaERF2 positively regulate artemisinin biosynthesis in Artemisia annua L. In *Molecular Plant*. pp. 353–365.

Zhang, H., Hedhili, S., Montiel, G., Zhang, Y., Chatel, G., Pré, M., Gantet, P. and Memelink, J. (2011) The basic helix-loop-helix transcription factor CrMYC2 controls the jasmonate-responsive expression of the ORCA genes that regulate alkaloid biosynthesis in Catharanthus roseus. *Plant J.*, **67**, 61–71.

Zhou, Y., Sun, W. and Chen, J. (2016) SmMYC2a and SmMYC2b played similar but irreplaceable roles in regulating the biosynthesis of tanshinones and phenolic acids in Salvia miltiorrhiza. *Sci Rep*, **6**, 22852.

Zi, J., Mafu, S. and Peters, R.J. (2014) To gibberellins and beyond! Surveying the evolution of (di)terpenoid metabolism. *Annu. Rev. Plant Biol.*, **65**, 259–286.

Zi, J., Matsuba, Y., Hong, Y.J., Jackson, A.J., Tantillo, D.J., Pichersky, E. and Peters, R.J. (2014) Biosynthesis of lycosantalonol, a cis -prenyl derived diterpenoid. *J. Am. Chem. Soc.*, **136**.

Figure legends:

Figure 1 Characteristic of *A. paniculata* plant

(A) Plant growth habit

(B) Close-ups of leaf and flower

Figure 2 Evolution of the *A. paniculata* genome

(A) Venn diagram of shared orthologous gene families among 4 species, i.e. *S. lycopersicum*, *V. vinifera*, *S. indicum* and *A. paniculata*.

(B) Proportion of orthologous genes in 12 plant genomes.

(C) Estimation of the time of divergence (with error range shown in parentheses) of *A. paniculata* and eleven other species based on orthologous single-copy gene pairs. Stars highlight the location of WGD events.

(D) Expansion and contraction of gene families among 12 plant genomes. Pie diagram on each branch and node corresponds to combined change across lineages. Mgut, *M. guttatus*; Sind, *S. indicum*; Apan, *A. paniculata*; Ugib, *U. gibba*; Slyc, *S. lycopersicum*; Vvin, *V. vinfera*; Gmax, *G. max*; Atha, *A. thaliana*; Ptri, *P. trichocarpa*; Osat, *O. sativa*; Zmay, *Z. mays*.

Figure 3 A general proposed pathway for diversified diterpenoid scaffolds and the major constituents andrographolide and neoandrographolide. Five diterpene synthases including CPS1-3 (CPS2 previously characterized) and KSL1-2 form distinct diterpene scaffolds. A proposed biosynthesis of andrographolide, neoandrographolide and other labdane diterpenoids based on known compounds from *A. paniculata* is represented. *Ent*-copalol intermediates are further modified by cytochromes P450 and other enzyme classes to afford the array of specialized diterpenoids.

Figure 4 Functional and stereochemical analysis of *ApCPS*s and *ApKSL*s.

(A) Phylogenetic analysis of the CPS and KSL genes in different plants. Neighbor-joining trees of class II and class I diterpene synthases based on aligned protein sequences. The phylogenetic tree was rooted with JsCPSKS and PpCPS/KS. Protein sequences are shown in Table S12. (B) Production of CPP (of either *ent*- and/or normal stereochemistry). GC-MS chromatograms of extracts from cultures expressing ApCPS1 or 3 (as indicated) in *E. coli* also engineered to produced GGPP. CPP is detected as the dephosphorylated copalol, presumably generated by endogenous phosphatases, with verification by comparison of retention time and mass spectra to an extract from a strain analogously engineered with a known CPS. (C) ApCPS1 produces both *ent*- and normal CPP. GC-MS chromatograms of extracts from cultures in which ApCPS1 is expressed in *E. coli* also engineered to produce GGPP and additionally co-expressing either the normal CPP specific AS or *ent*-CPP specific KS, with comparison to CPSs of known stereospecificity. (D) ApCPS3 produces normal CPP. GC-MS chromatograms of extracts from cultures in which ApCPS1 is expressed in *E. coli* also engineered to produce GGPP and additionally co-expressing the normal CPP specific AS, again with verification by comparison to an extract from an analogously engineered strain with CPS known to produce normal CPP. (E) ApKSL1 is specific for normal CPP and produces the same mixture of

abietadienes as AS. GC-MS chromatograms of extracts from cultures expressing ApKSL1 or AS in *E. coli* also engineered to produce CPP. (F) ApKSL2 readily reacts with *ent*-CPP. GC-MS chromatograms of extracts from cultures expressing ApKSL1 or KS in *E. coli* also engineered to produce *ent*-CPP. (G) ApKSL2 also reacts with normal CPP. GC-MS chromatograms of extracts from cultures expressing ApKSL1 or AS in *E. coli* also engineered to produce CPP.

Figure 5 Characterization of rApUGT73AU1 to Catalyze Andrograpanin to Neoandrographolide.

(A) The expression level of ApUGT73AU1 and the Neoandrographolide (Nap) content in seedlings after MeJA treatment. (B) Multiple sequence alignment of PSPG motifs of ApUGTs and SrUGTs. (C) Representative UPLC analysis showing the in vitro production of Neoandrographolide (Nap) by incubating rApUGT73AU1 with Andrograpanin (Nap-A). (D) Representative indicate the mass spectrum of Nap (upper panel) and Andrograpanin (Nap-A) for rApUGT73AU1. (E) The proposed pathway for Nap biosynthesis based on the functions of rApUGT73AU1.

Table legends:

Table 1 Summary of genome assembly

Table 2 The contents of diterpenoids in *A. paniculata* seedlings after treatment with MeJA

Table 1: Summary of genome assembly

Number of contigs	1278
Total contigs length	269306334
Longest contig	2074285
Shortest contig	4221
Contigs > 10K nt	1271 (99.45 %)
Contigs > 100K nt	737 (57.67 %)
Contigs > 1M nt	23 (1.80 %)
N50	388864
L50	208
N80	165327
L80	522
GC content	0.3332

Table 2: The contents of diterpenoids in *A. paniculata* seedlings after treated with MeJA

Main compounds (mg/g)	**0**	**24**	**48hs**
Andrographolide	0.326(0. 095)	0.779(0. 305)	0.868 (0. 252)
Andropanolide	0.959(0. 54)	1.532(0. 689)	2.328(0. 681)
14-Deoxyandrographolide	1.990(0. 133)	3.443(0. 358)	3.117 (0. 203)
Minor compounds (μg/g)			
Neoandrographolide	7.785(0. 54)	37.402(4. 72)	36.115(2. 484)
Andrograpanin	0.277(0. 092)	0.413(0. 286)	0.531(0. 113)
Andropanoside	27.327(0. 759)	72.775(14. 096)	71.067(7. 793)
14-Deoxy-11-hydroxyandrographolide	19.536(1. 417)	28.067(6. 216)	20.297(1. 103)
14-Deoxy-17-hydroxyandrographolide	3.629(0. 066)	5.569(1. 454)	4.69(1. 114)
14-Deoxy-11,12-dideroxyandrographoside	0.024(0. 005)	0.033(0. 002)	0.034(0. 0206)

Figure 1 Characteristic of *A. paniculata* plant

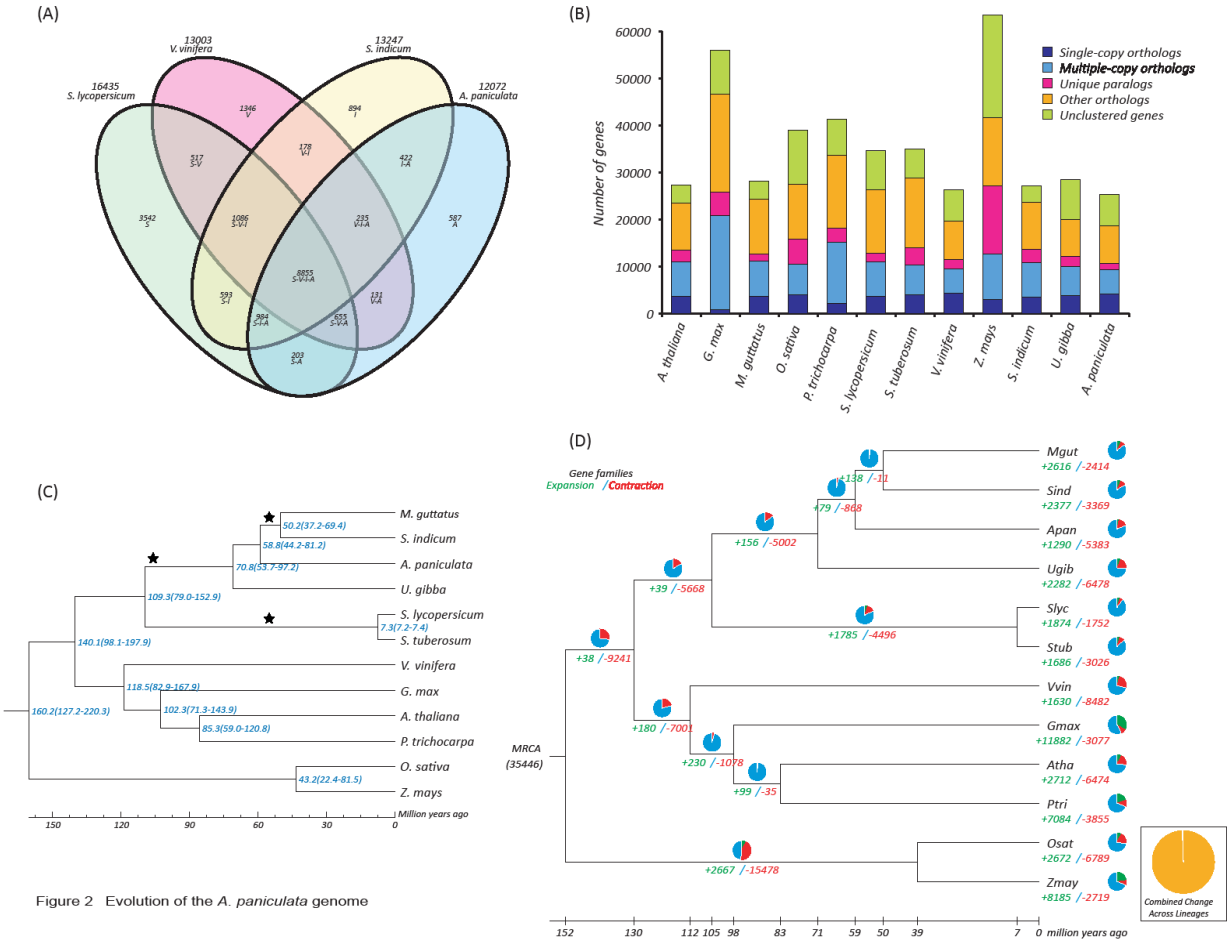

Figure 2 Evolution of the *A. paniculata* genome

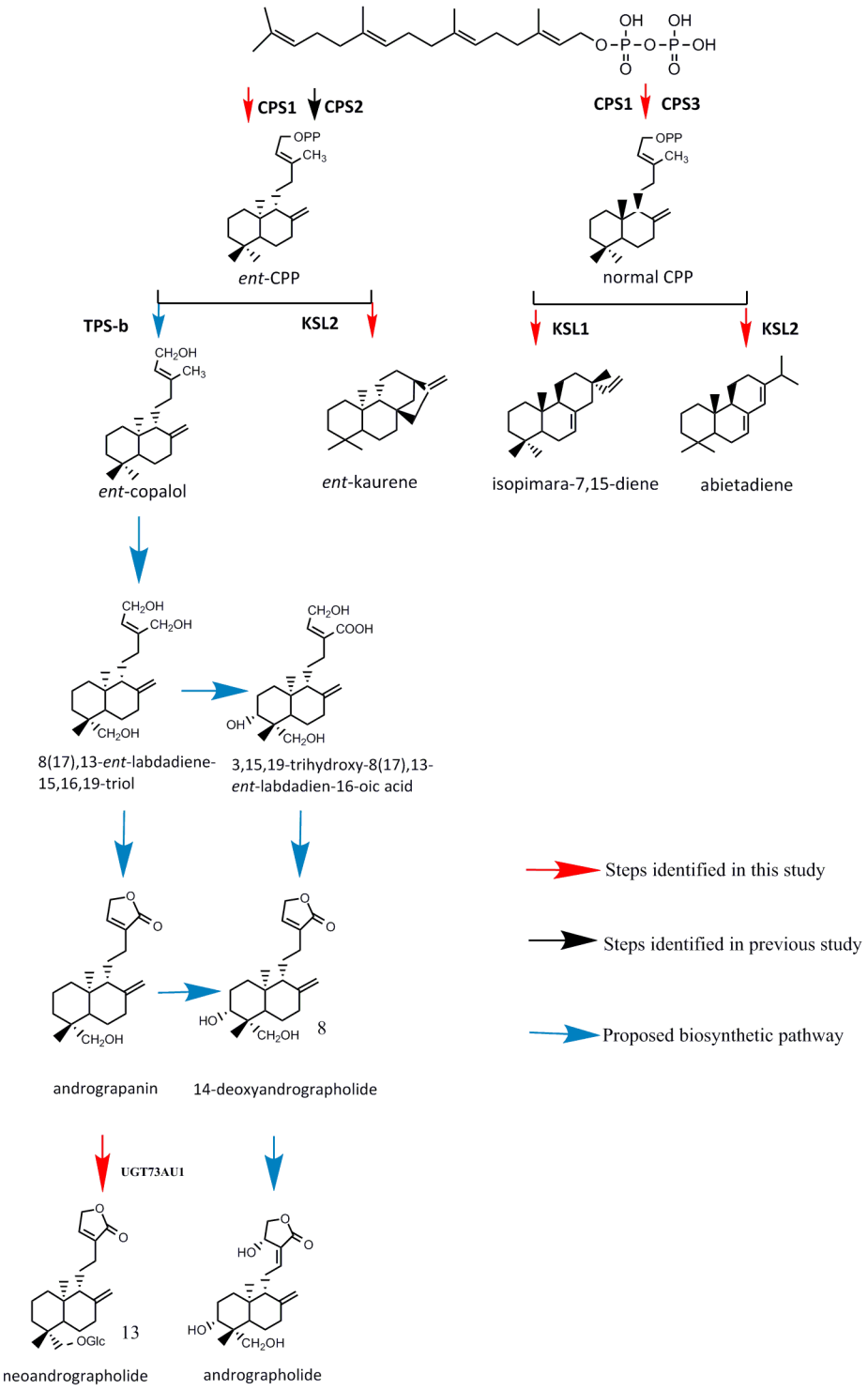

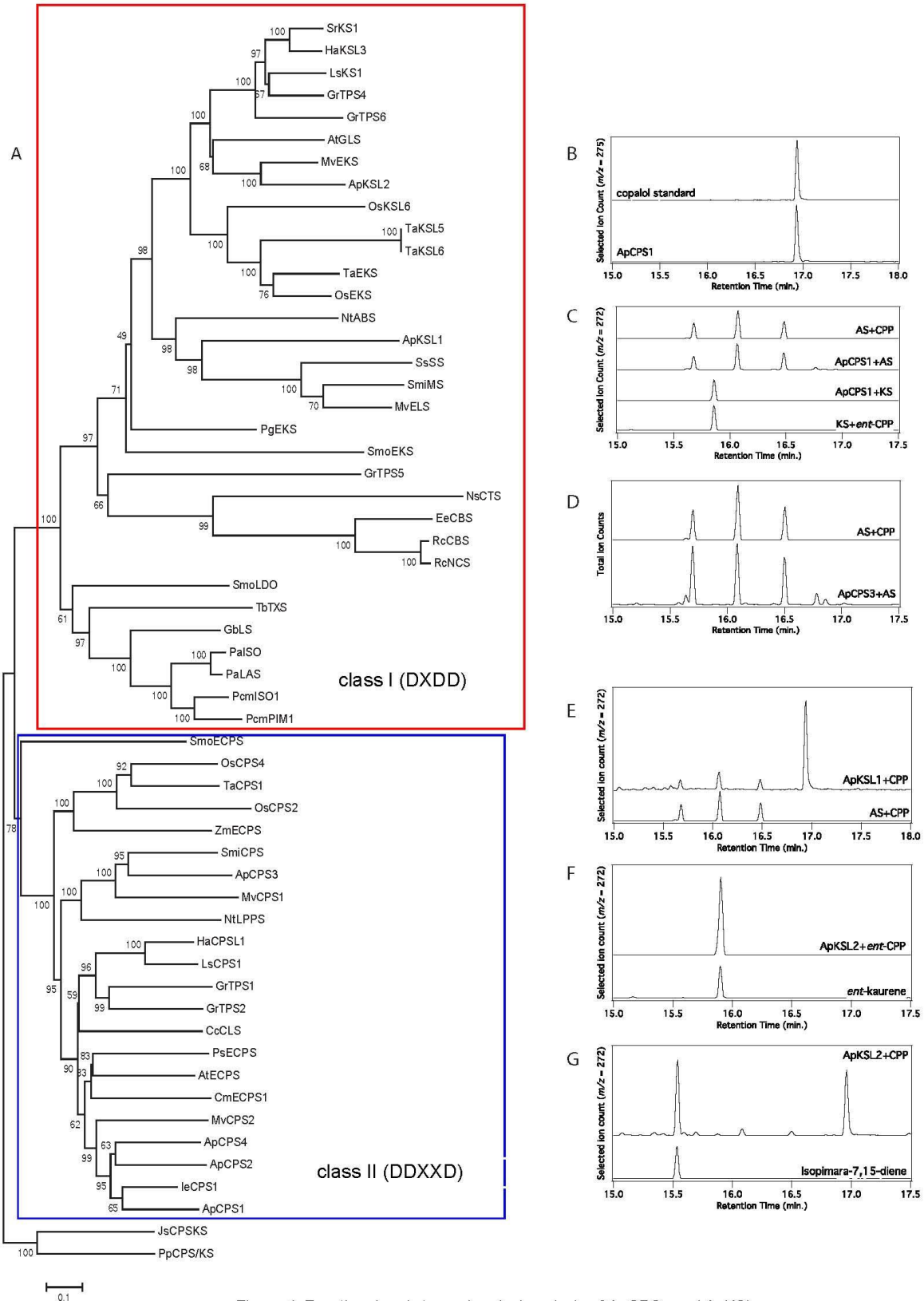

Figure 4 Functional and stereochemical analysis of ApCPSs and ApKSLs

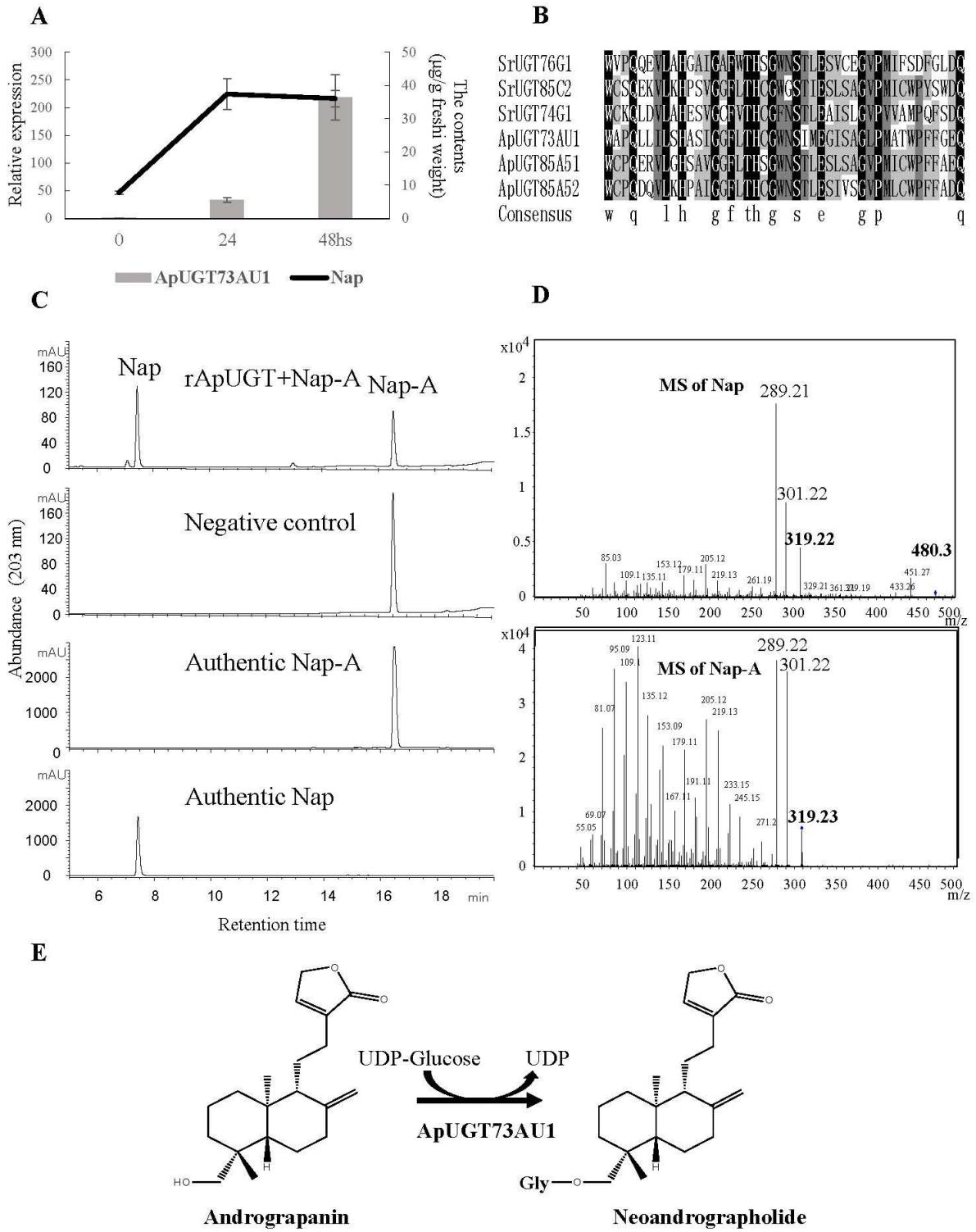

Figure 5 Characterization of rApUGT73AU1 to Catalyze Andrograpanin to Neoandrographolide